

带格式的: 两端对齐

1  
2  
3 **Carbon emission reduction requires attention to the contribution of natural gas use:**  
4 **Combustion and leakage**

5 Haoyuan Chen<sup>1,5</sup>, Tao Song<sup>1,5\*</sup>, Xiaodong Chen<sup>2</sup>, Yinghong Wang<sup>1</sup>, Mengtian Cheng<sup>1</sup>, Kai  
6 Wang<sup>1</sup>, Fuxin Liu<sup>4</sup>, Baoxian Liu<sup>3</sup>, Guiqian Tang<sup>1,5\*</sup>, Yuesi Wang<sup>1,5</sup>

7 Correspondence to Guiqian Tang (tgq@dq.cern.ac.cn) Tao Song (st@dq.cern.ac.cn)

8 1. Key Laboratory of Atmospheric Environment and Extreme Meteorology, Institute of

9 Atmospheric Physics, Chinese Academy of Sciences, Beijing, China

10 2. Beijing Aozuo Ecological Instrument Co., Ltd., Beijing 100080, China

11 3. Beijing Key Laboratory of Airborne Particulate Matter Monitoring Technology, Beijing

12 Municipal Environmental Monitoring Center, Beijing, 100048, China

13 4. Anhui University of Science and Technology, Anhui 232001, China

14 5. University of Chinese Academy of Sciences, Beijing 100049, China

15 Abstract: Natural gas will continue to replace coal in the process of global energy structure reform,  
16 but its leakage potential can delay the realization of global carbon neutrality. To quantify its impact,  
17 we established a carbon dioxide (CO<sub>2</sub>) and methane (CH<sub>4</sub>) flux detection platform on the 220-m  
18 platform of the Institute of Atmospheric Physics, Chinese Academy of Sciences, located in  
19 northwestern Beijing. The observation results indicated that the daily mean CO<sub>2</sub> and CH<sub>4</sub> fluxes  
20 were  $12.21 \pm 1.75 \mu\text{mol} \cdot \text{m}^{-2} \cdot \text{s}^{-1}$  and  $95.54 \pm 18.92 \text{ nmol} \cdot \text{m}^{-2} \cdot \text{s}^{-1}$ , respectively. The fluxes were  
21 significantly correlated with natural gas consumption, indicating that natural gas has become a  
22 common source of CH<sub>4</sub> and CO<sub>2</sub>, the combustion of which releases CO<sub>2</sub>, while its leakage processes  
23 emit CH<sub>4</sub>. Vehicle-based identification demonstrated that CH<sub>4</sub> can escape at the production, storage  
24 and use stages of natural gas. Based on natural gas consumption data, the upper limit of the  
25 calculated natural gas leakage rate in Beijing reached  $1.12\% \pm 0.22\%$ , indicating that the  
26 contribution of CH<sub>4</sub> to climate change could reach 23 % of that of CO<sub>2</sub> on a 20-year scale. Natural  
27 gas leakage was estimated to delay the time for China to achieve carbon neutrality by at least almost  
28 four years.

29 **KEY WORDS:**

30 CO<sub>2</sub> flux, CH<sub>4</sub> flux, Eddy covariance, Natural gas leakage, Climate forcing, Carbon neutrality

31 **1. INTRODUCTION**

32 In 2015, the 1.5 °C temperature control target was proposed in the Paris Agreement to reduce  
33 the occurrence of extreme weather events(Seneviratne et al., 2018). To achieve this goal, it is  
34 necessary to actively promote the low-carbon development transformation of the economic system,  
35 especially energy transformation. In this process, natural gas plays an important role, and typical  
36 countries have indicated a trend of coal reduction and gas increase during energy structure  
37 adjustment over the past century. It is expected that global natural gas consumption will continue to  
38 increase by 2035.

39 Natural gas is commonly referred to as a clean alternative to coal, but its main component is  
40 methane, with a global warming potential (GWP) that is 29.8 times greater than that of carbon  
41 dioxide at the hundred-year scale(Environmental-Protection-Agency, 2024). If 3.4 % of methane  
42 leaks into the atmosphere before natural gas combustion, the advantages of natural gas over coal  
43 will become negligible(Kemfert et al., 2022). Recent studies have suggested that the average loss  
44 rate of natural gas in cities worldwide ranges from 3.3 % to 4.7 %(Sargent et al., 2021). According  
45 to statistics from the International Energy Agency ([www.iea.org](http://www.iea.org)) in 2020, methane leakage in the  
46 global oil and gas industry reached 72 million tons and amounted to 6 billion tons of carbon dioxide  
47 equivalent (CO<sub>2</sub>e) within 20 years. Therefore, it is unclear whether natural gas can become a  
48 bridging material for energy transformation.

49 One important prerequisite is to determine the contribution of natural gas leakage during coal-  
50 to-gas conversion to urban methane (CH<sub>4</sub>) emissions and its climate effects. At present, conventional  
51 CH<sub>4</sub> monitoring methods include ground, aviation, and satellite monitoring methods. Ground  
52 monitoring aims to detect the atmospheric CH<sub>4</sub> concentration through the installation of sensors and  
53 monitoring stations at fixed locations or on vehicles(Wunch et al., 2016). Notably, monitoring  
54 equipment is often installed near potential emission sources, with high detection accuracy but  
55 generally a limited spatial range. The aviation monitoring method can be employed to identify large-  
56 scale CH<sub>4</sub> emissions through measurement techniques such as drones or aircraft but cannot be used  
57 to achieve long-term monitoring(Duren et al., 2019; Frankenberg et al., 2016; Sherwin et al., 2024).  
58 Satellite methods can compensate for the shortcomings of the former two methods(Chen et al., 2022;  
59 Cusworth et al., 2018; Shen et al., 2023), which exhibit interference from clouds and require  
60 significant labor and financial investments.

61 The eddy covariance method, which is based on tall towers, enables long-term monitoring of  
62 methane emissions, thus facilitating the identification of methane sources in specific areas. However,  
63 it should be noted that this method has certain limitations during urban flux measurements at higher  
64 altitudes, as larger air volumes in the measurement system may lead to a significant imbalance  
65 between the observed vertical turbulence exchange and surface net flux compared with those at  
66 typical measurement heights. However, this deficiency should be considered in conjunction with  
67 the advantages of urban tower measurements because cities typically correspond to deeper rough  
68 sublayers that can extend to 2–5 times the average building height(Barlow, 2014). Therefore,  
69 increasing the measurement altitude can help characterize the turbulent exchange between this layer  
70 and the inertial sublayer.

71 Developing countries are the main driving force behind the continuous growth in global energy  
72 demand. As Beijing is the capital of the world's largest developing country and the first city within  
73 China to complete the coal-to-gas conversion process, clarifying the natural gas leakage process in  
74 Beijing can provide guidance for energy transformation in developing countries regionally and even  
75 globally. In this study, three aspects related to natural gas were investigated as follows. First, the  
76 fluxes of  $\text{CH}_4$  and  $\text{CO}_2$  were observed simultaneously via the eddy covariance method, which was  
77 used to investigate the impact of the coal-to-gas policy on  $\text{CO}_2$  and  $\text{CH}_4$  in Beijing, including the  
78 magnitude of  $\text{CO}_2$  emission and the common effects on the sources of both. Second, with navigation  
79 experiments, the natural gas leakage process in Beijing has been confirmed, and the emission levels  
80 of natural gas at different stages have been further roughly estimated, which provides certain  
81 effective insights for the control of natural gas leakage in Beijing. Third, we discuss climate forcing  
82 caused by natural gas leakage while considering the  $\text{CO}_2$  flux as a basis, calculate the natural gas  
83 leakage rate with statistical data, and estimate the impact of natural gas leakage on China's carbon  
84 peak and carbon neutrality in conjunction with existing reports.

85

带格式的: 缩进: 首行缩进: 0 字符

## 86 2. METHODS

### 87 2.1 Instrument setup for eddy covariance measurement

88 The measurements were conducted at a 325-m high meteorological tower in northwestern  
89 Beijing, with a closed-path observation system installed on a platform at a height of 220 m, which

90 included a dual laser gas analyzer (QC-TILDAS-DUAL, Aerodyne Research Inc., USA), three-  
91 dimensional ultrasonic anemometer (Gill Instruments, Ltd., Lymington, Hampshire, UK), vacuum  
92 pump (XDS35i, BOC Edwards, UK), data collector (CR6, Campbell Scientific Inc., USA), and  
93 other accessories. In the dual laser gas analyzer, tunable infrared laser direct absorption spectroscopy  
94 (TILDAS) technology is used to detect the most significant fingerprint transition frequencies of  
95 molecules within the mid-infrared wavelength range. The analyzer has an optical path of up to 76  
96 m and can measure  $\text{H}_2\text{O}$ ,  $\text{CO}_2$  and  $\text{CH}_4$  simultaneously. Similar instruments have been applied to  
97 observe outdoor ecosystems (Zöll et al., 2016). Under the action of a vacuum pump, the air sample  
98 enters the instrument room at a flow rate of 2 lpm through a polytetrafluoroethylene sampling tube  
99 with a length of 3 m and an inner diameter of 3 mm (Figure S1). Instrument calibration includes  
100 zero-point and range calibration processes. High-purity nitrogen gas (>99.999%) was used for zero-  
101 point calibration at 1-hour intervals. In this process, the corresponding solenoid valve was opened,  
102 which was automatically controlled by TDLWintel software, and range calibration was performed  
103 at the factory. In addition, before the experiment, we calibrated the gas analyzer using  $\text{CO}_2$  (401  
104 ppm) and  $\text{CH}_4$  (2190 ppb) standard gases. We found that the measured and standard gas  
105 concentrations differed by less than 1%, indicating satisfactory instrument performance. Therefore,  
106 we did not perform range calibration later. The instrument was placed in an insulated box equipped  
107 with air conditioning to ensure normal operation of the laser. Both instruments were operated at a  
108 sampling frequency of 10 Hz. The data collector and high-frequency instrument were timed  
109 according to the network and global positioning system (GPS), respectively, to maintain  
110 synchronization. To minimize the twisting effect of the flux tower on the incoming air, a three-  
111 dimensional ultrasonic anemometer was installed at the end of a 1.5-m long support arm facing  
112 southeast China in summer. This measurement lasted from June 11 to September 7, 2022, during  
113 which the nitrogen cylinder was replaced, and the instrument was debugged on June 18 and 19.  
114 From July 12 to 26, the experiment was stopped due to failure of the tower power supply.

## 115 **2.2 Flux data processing**

116 The flux data processing operation in this study is based on the eddy covariance technique via  
117 EddyPro software (version 6.2.1, Li COR, Inc.; Lincoln, Nebraska, USA). An average flux  
118 calculation period of 30 minutes was selected (Lee, 2004). Before calculating half-hourly fluxes,

119 spike detection and data rejection algorithms were applied like follows as described by Vickers et  
120 al., (1997): Take a moving window with a width equal to 1/6 of the averaging period (typically 5  
121 minutes) and calculate the mean and standard deviation of the time series within the window. Define  
122 outliers as any data points deviating from the mean by n times the standard deviation (initial n =  
123 3.5). Replace the identified outliers with linearly interpolated values from adjacent points.  
124 Consecutive outliers  $\leq 3$  are treated as a single outlier; consecutive outliers  $\geq 4$  are considered local  
125 trends and excluded from outlier classification. Iteratively increase n by 0.1 per cycle until no  
126 outliers are detected or 20 iterations are reached. Advance the window by half its width (step size)  
127 and repeat outlier detection/removal for the next window. Continue this process until all outliers are  
128 processed within the averaging period. If outliers exceed 1 % of the total data points in any averaging  
129 period, discard that entire period.

130 The double rotation method proposed by Kaimal et al., (1994) was employed for tilt correction.  
131 The delay time caused by the spatial separation of gas analyzers and three-dimensional ultrasonic  
132 anemometers (as well as the injection pipeline of closed-path systems) was corrected via the  
133 maximum covariance method(Fan et al., 2012). Webb, Pearman, and Leuning (WPL) correction  
134 was not applied here(Webb et al., 2007) because the instrument room was in a state of constant  
135 temperature and pressure that converted the real-time concentration into a dry volume mixing ratio,  
136 and the longer pipeline of the closed-path system avoided the influence of temperature fluctuations.  
137 The limitations of eddy covariance systems can lead to frequency loss in flux observations. Factors  
138 such as a limited average period and linear detrending can cause low-frequency loss, whereas  
139 instrument separation, path averaging, insufficient high-frequency responses, and pipeline  
140 attenuation can cause high-frequency loss. The method proposed by Moncrieff et al., (1996) was  
141 employed for frequency response correction. After the above correction of the flux data, in this paper,  
142 the 0-1-2 quality labeling scheme proposed by Mauder and Foken(Mauder et al., 2004) was adopted  
143 for data quality control purposes. Notably, a value of 0 represents data with the best quality, a value  
144 of 1 represents data with good quality, and a value of 2 represents data with poor quality. In this  
145 study, flux data marked as 2 were excluded from the subsequent analysis. In addition, the flux source  
146 area was evaluated via the method of Kljun et al., (2004) (Text. S1), and the flux source area covered  
147 most of the urban area of Beijing and reflected the average emission characteristics of urban Beijing

148 (Figure S2).

149 **2.3 Spectral analysis**

150 High-frequency signal loss can occur in closed-path systems. To determine the response  
151 capability of the closed-path system to high-frequency turbulence signals, we analyzed the observed  
152 gas exchange signals through the turbulence power spectrum. The selected time ranges from 12:00  
153 to 16:00 every day during the observation period, with a total of 8 and a half hours of data. The data  
154 were integrated and averaged, and the data curve was then compared with the ideal slope in the  
155 inertia subarea (Figure S3).  $Co(wT)$  followed the theoretical  $f_n^{-4/3}$  (where  $f_n$  denotes the normalized  
156 frequency) in the inertial subregion. In contrast, the slopes of  $Co(wCO_2)$  and  $Co(wCH_4)$  were  
157 slightly greater than  $-4/3$ , indicating that there was high-frequency loss in the flux observations of  
158 the closed-loop system (Kaimal et al., 1972). Through high-frequency correction, the calculation  
159 results indicated that the  $CO_2$  and  $CH_4$  fluxes were 7.73 % and 6.85 % greater, respectively, than  
160 those before correction.

161 **2.4 Mobile  $CH_4$  and  $CO_2$  observations**

162 Vehicle-based experiments were conducted in the urban area of Beijing in the winter of 2023  
163 and the summer of 2024, and the specific deployment of the mobile observation station is shown in  
164 Figure S1. Notably, the car was equipped with a  $CO_2/CH_4$  spectrometer (Los Gatos Research, Inc.,  
165 USA), a laptop for data viewing, and a mobile power supply (Figure S4). Zero-point calibration of  
166 the instrument was performed once pure nitrogen was used before the mobile experiment began.  
167 Standard gases of methane and carbon dioxide were introduced to calibrate the instrument  
168 simultaneously, and we found that the concentration of the instrument matched well with the  
169 standard gas. Since we focused more on the enhancement in concentration rather than itself, we did  
170 not calibrate it again afterward. The sampling port was located approximately 20 cm from the roof,  
171 and ambient air was collected through a PTFE tube with a length of 2 m and an inner diameter of 3  
172 mm. Before the particulate matter entered the instrument, it was removed using a filter head. The  
173 IMET sounding instrument (International Met Systems, USA) is installed on the roof, with a  
174 sampling frequency that is consistent with that of the other instruments, i.e., 1 s, real-time  
175 concentration information of different latitudes and longitudes is obtained at a resolution of seconds  
176 through the corresponding time between the GPS and the instrument; for example, if the GPS

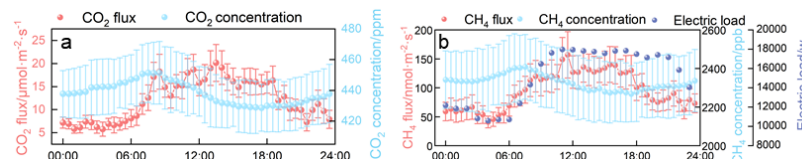
177 sampling time delay is 3 s, the latitude and longitude coordinates are reassigned to the CH<sub>4</sub> reading  
178 observed three seconds prior. Our observation sites include petrochemical plants located in  
179 southwestern Beijing, natural gas storage tanks and landfills in the northeastern part, and power  
180 plants with the highest natural gas usage in the southeastern part.

181 **3. RESULTS**

182 **3.1 Diurnal variation in the flux**

183 A positive or negative flux reflects the vertical exchange direction of trace gases in the urban  
184 canopy, which is positive upward and negative downward. (The uncertainty analysis is described in  
185 the Text, S2 and Figure S5, respectively) Overall, both CO<sub>2</sub> and CH<sub>4</sub> fluxes are positive on a daily  
186 scale, indicating that cities are the source of both gases. The diurnal CO<sub>2</sub> flux ranged from 6.05 to  
187 19.66  $\mu\text{mol}\cdot\text{m}^{-2}\cdot\text{s}^{-1}$  with an average of  $12.21 \pm 1.75 \mu\text{mol}\cdot\text{m}^{-2}\cdot\text{s}^{-1}$  (Figure 1a), which was generally  
188 lower than the summer observations by Cheng et al., (2018) and Liu et al., (2012) at 200 m and 140  
189 m at this tower, respectively (Table S1), a smaller deviation suggests that CO<sub>2</sub> may be dominated by  
190 a more stable source than before. We also obtained observation results at 140 m in summer from  
191 2009–2017 (Liu et al., 2020). The flux in 2022 significantly decreased compared with previous  
192 levels (Figure S6), which reflects the transformation of Beijing's energy structure. The coal-to-gas  
193 policy implemented by Beijing these years led to a gradual decrease in the proportion of coal in  
194 primary energy consumption, with a steady increase in the proportion of natural gas in total  
195 consumption (Figure S7), the use of natural gas results in much less coal CO<sub>2</sub> than coal, generating  
196 the same amount of heat; moreover, Beijing has increased the amount of electricity flow from other  
197 provinces in recent years (Figure S7), which has further driven a decrease in the annual average  
198 concentration of PM<sub>2.5</sub>, dropping to 30.5  $\mu\text{g}\cdot\text{m}^{-3}$  by 2024. In fact, previous studies have reported a  
199 high correlation between PM<sub>2.5</sub> and CO<sub>2</sub> fluxes. For example, Donateo et al., (2019) found that the  
200 seasonal and daily variations in the particle number flux in southern Italian suburbs are largely  
201 determined by both transportation activities and household heating. Liu et al., (2020) confirmed that  
202 the CO<sub>2</sub> flux can explain 64 % of the interannual variation in the PM<sub>2.5</sub> concentration by fitting the  
203 correlation between the annual average PM<sub>2.5</sub> and CO<sub>2</sub> fluxes in Beijing from 2009 to 2017.  
204 Therefore, controlling CO<sub>2</sub> emissions can also greatly control the concentration level of PM<sub>2.5</sub>,  
205 thereby achieving the dual effects of mitigating climate change and improving air quality. In terms

206 of its diurnal variation, it did not follow a typical bimodal pattern but rather remained high after  
 207 reaching the first peak at 8:00, with a lower level at night, reflecting high anthropogenic carbon  
 208 emissions during the day, such as those resulting from transportation and energy generation  
 209 activities. The diurnal pattern of the  $\text{CH}_4$  flux was similar to the observation results of Giolo et al.,  
 210 (2012) and Helfer et al., (2016) (Figure 1b), reflecting an increase in emissions during the day. The  
 211  $\text{CH}_4$  flux began to increase gradually from 04:00 to around 08:30, and then remained stable until  
 212 after 10:30, when it began to rise rapidly again, reaching its daily peak of approximately 157.1 nmol  
 213  $\text{m}^{-2} \text{ s}^{-1}$  around 11:30. After 17:30, it slowly declined. Its diurnal variation pattern showed some  
 214 differences compared to  $\text{CO}_2$  flux, which increased beginning at 03:30 to around 08:30 similar to  
 215  $\text{CH}_4$  flux. However, the peak for  $\text{CO}_2$  flux occurred around 13:30, then slowly decreased and  
 216 decreased rapidly after 18:30. Assuming that the average  $\text{CH}_4$  flux at midnight (00:00 to 06:00) can  
 217 be employed as the baseline for nighttime emissions, it accounted for 58% of the daily average flux.  
 218 The  $\text{CH}_4$  flux demonstrated a pronounced diurnal pattern, indicating a significant daily variation in  
 219 the background source in the source area.



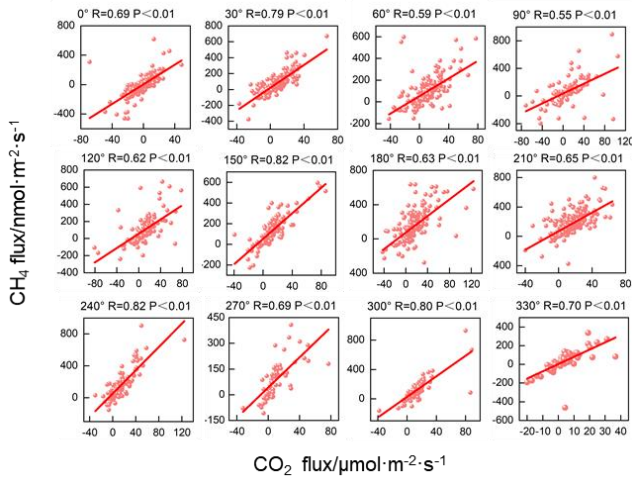
220 Figure 1 Daily variations in the  $\text{CO}_2$  and  $\text{CH}_4$  concentrations, fluxes, and electricity loads

221 **Figure 1 Daily variations in the  $\text{CO}_2$  and  $\text{CH}_4$  concentrations, fluxes, and electricity loads**

### 222 **3.2 Homology between $\text{CO}_2$ and $\text{CH}_4$**

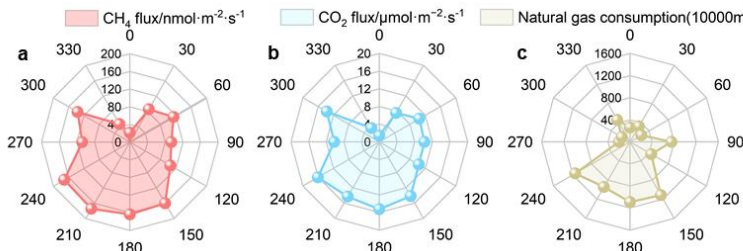
223 The  $\text{CO}_2$  and  $\text{CH}_4$  fluxes showed a significant correlation along all directions (Figure 2), with  
 224 correlation coefficients greater than that at the center of Loz, Poland (0.50) (Pawlak et al., 2016), but  
 225 the low correlation between the  $\text{CO}_2$  and  $\text{CH}_4$  fluxes and the temperature excludes the conclusion  
 226 that biological sources dominate their emissions (Figure S8). Therefore,  $\text{CO}_2$  and  $\text{CH}_4$  share the  
 227 same anthropogenic sources within the source area. This homology is also reflected in their spatial  
 228 distributions, with high fluxes distributed mainly south of the tower, which is more densely  
 229 populated and encompasses complex industrial structures, and much lower fluxes in the northern  
 230 forest and park areas (Figure 3a, b). The correlation between the spatial distributions of the  $\text{CO}_2$  and  
 231  $\text{CH}_4$  fluxes is high (Figure 3c). The correlation coefficient between the  $\text{CO}_2$  and  $\text{CH}_4$  fluxes is 0.75, and  
 232 the correlation coefficient between the  $\text{CO}_2$  and  $\text{CH}_4$  concentrations is 0.72.

233 CH<sub>4</sub> fluxes reached 0.98, demonstrating the common impact of similar anthropogenic sources on  
 234 their emissions. The linear fitting results at 150° and 240° indicated the highest correlation  
 235 coefficient (0.82) along all directions (Figure 2), further supporting this viewpoint.



236

237 Figure 2 Linear fitting results for the 30-minute CH<sub>4</sub> and CO<sub>2</sub> fluxes in the 12 directions



238

239 Figure 3 Mean CH<sub>4</sub> and CO<sub>2</sub> concentrations, fluxes and natural gas consumption in the 12  
 240 directions

241

#### 242 4. DISCUSSION

##### 243 4.1 Driver of the homology between CO<sub>2</sub> and CH<sub>4</sub>

244 After the introduction of natural gas in 1985, the proportion of natural gas in the fossil fuel  
 245 industry of Beijing increased annually, especially when coal was replaced with natural gas and  
 246 electricity in 2014 and 2018, respectively, and natural gas became the most consumed fossil fuel  
 247 (Figure 6a). According to the 2022 Beijing Statistical Yearbook

248 (<https://nj.tjj.beijing.gov.cn/nj/main/2023-tjnjk/e/indexch.htm>), natural gas is used mainly for  
249 thermal power generation and heating (accounting for 69 %). Owing to the low proportion of heating  
250 in summer, natural gas in Beijing is mostly used for thermal power generation in summer. Owing to  
251 the difficulty in obtaining hourly electricity generation data, we obtained a daily variation curve of  
252 the electricity load in Beijing based on the statistical data (power plants usually calculate the  
253 required electricity generation based on the electricity load) (<https://www.gov.cn/xinwen/2019-12/30/5465088/files/e3682ce168c8427b886a43a790d66c2c.pdf>) (Figure 1b). The daily variation in  
254 the electricity load is highly consistent with that in the CH<sub>4</sub> flux, with the maximum CH<sub>4</sub> flux  
255 occurring at 11:00 pm during the peak electricity consumption period. After 16:00 pm, the electricity  
256 load and CH<sub>4</sub> flux decrease synchronously. Thus, the daily variation in the CH<sub>4</sub> flux is driven by  
257 natural gas consumption. We gridded the natural gas consumption data (Figure S9) and calculated  
258 the mean natural gas consumption along all directions within the flux source area (Figure 3c).  
259 Notably, a high consistency between the spatial distributions of the CO<sub>2</sub> and CH<sub>4</sub> fluxes and natural  
260 gas consumption was found, which reflects that after the adjustment of the energy structure in  
261 Beijing, natural gas became the main source of CO<sub>2</sub> and CH<sub>4</sub>. Considering the high photosynthetic  
262 absorption of CO<sub>2</sub> by plants in summer, this conclusion also applies to the other seasons, which  
263 supports the hypothesis that natural gas is the main source of winter CO<sub>2</sub> emissions in Beijing, as  
264 determined based on the isotope tracing method(Wang et al., 2022; Wang et al., 2022).

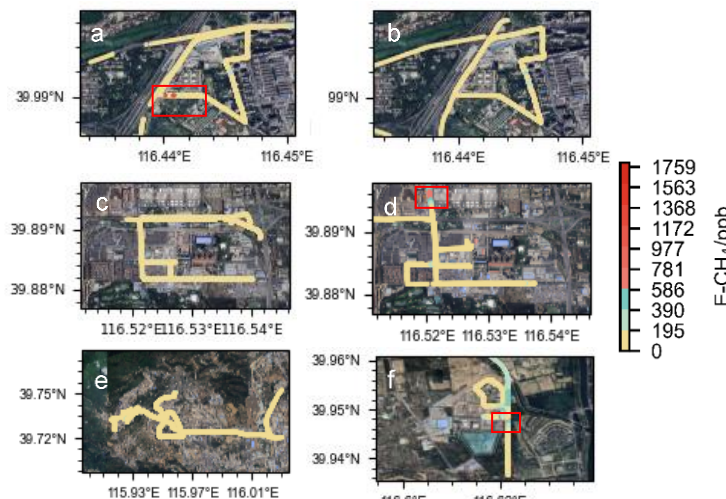
266 To verify this conclusion and identify the primary phases of natural gas leakage, we conducted  
267 mobile observations during winter and summer around large petrochemical plants, gas storage tanks,  
268 and power plants in Beijing. Given real-time variations in gas concentrations influenced by  
269 meteorological conditions and pollution transport, it was essential to determine background  
270 concentrations at each time point. The current mainstream approach for determining background  
271 values involves calculating the 5<sup>th</sup> or 10<sup>th</sup> percentile within a sliding window of 5 minutes ( $\pm$  2.5  
272 min) or 10 minutes ( $\pm$  5 min) centered on the target timestamp (Pu et al., 2023, Well et al., 2018;  
273 Well et al., 2019). We compared and evaluated the results applying different combinations of time  
274 windows or percentile following the method of Schiferl et al., (2025). (Text. S3). The 10-min time  
275 window with 5<sup>th</sup> percentile was used here to calculate the background value. The enhancement  
276 concentration can be defined as the difference between the observed value and the background value

277 at the corresponding time. There was significant CH<sub>4</sub> leakage around the gas storage tanks and  
278 power plants in both winter and summer. Notably, the observed CH<sub>4</sub> hotspots were located in the  
279 downzone of potential leakage sources; therefore, we attribute the high CH<sub>4</sub> concentration to the  
280 emissions of these potential natural gas leakage sources. In winter, hotspots with concentrations  
281 higher than the background value of 1759 ppb appeared around the gas storage tank (Figure 4a),  
282 corresponding to an enhancement concentration of CH<sub>4</sub> (E-CH<sub>4</sub>) and enhancement concentration of  
283 CO<sub>2</sub> (E-CO<sub>2</sub>) fingerprint line with a slope of 0.11 (Figure 5a). In addition, the enhancement  
284 concentration fingerprint slopes of the other hotspot zones were 0.06 and 0.07, respectively,  
285 indicating varying degrees of leakage around the gas storage tank(Sun et al., 2019).The  
286 enhancement concentration fingerprint in summer also revealed leakage related to gas storage  
287 equipment (Figure 4b), with a slope of 0.04, analogous to that of 0.06 in winter. Similar to gas  
288 storage tanks, natural gas leakage hotspots have been observed in various equipment in power plants.  
289 For example, fingerprints with a slope of 0.005 (Figure 5d) in summer reflected leakage related to  
290 combustion devices or pipeline in power plants(Lamb et al., 1995), whereas fingerprints with a slope  
291 of 0.015, 0.02 or 0.05 reflected leakage related to storage facilities (Figure 5c,d)(Hurry et al., 2016).  
292 We also discovered natural gas leakage near the petrochemical plant (Figure 4e), the line with a  
293 slope of 0.02 was related to the gas storage equipment, and the line with a slope of 0.005 was  
294 relevant to the natural gas combustion equipment. As important sources of methane, landfills have  
295 received widespread attention, so we also conducted mobile observations near a large landfill  
296 outside the Fifth Ring Road in Beijing, which was a hotspot exhibiting a level exceeding the  
297 minimum concentration of 1375 ppb (Figure 4f). The concentration fingerprints were relatively  
298 disordered and significantly differed from those of CH<sub>4</sub> emissions dominated by natural gas (Figure  
299 5f), indicating that waste disposal processes are relatively complex and cannot be ignored in  
300 cities(Cusworth et al., 2024).

301 Converting observed concentration increments into emission rates is a simple means of  
302 quantifying natural gas leakage, which is subject to atmospheric conditions and potential leak source  
303 locations. Weller et al., (2018; 2019) developed a model based on the relationship between the  
304 enhancement concentration and emission rate. The specific formula is shown in Text S4. The model  
305 assumes that CH<sub>4</sub> enhancement is the best predictor of the leakage emission rate and that a greater

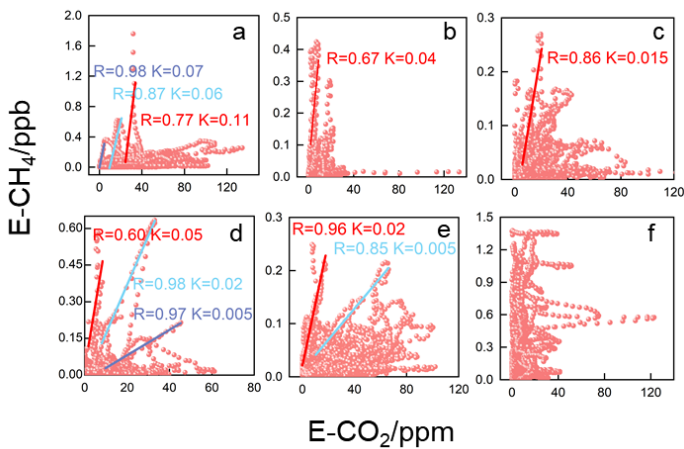
306 leakage emission rate corresponds to greater  $\text{CH}_4$  enhancement. The method sets a minimum  
 307 threshold for the observed  $\text{CH}_4$  concentration, which is 110 % of the background value, to filter out  
 308 concentration changes caused by measurement. Moreover, when multiple detections are conducted  
 309 for the same leakage source, it is necessary to average the  $\text{CH}_4$  enhancement values and then  
 310 substitute them into the above formula. We estimated the natural gas leakage emission rates from  
 311 different leakage sources with this method, and the confidence interval (CI) based on the Bootstrap  
 312 method was used to estimate the uncertainty of the leakage rate. The natural gas leakage rate from  
 313 the gas storage tank and power plant in winter were  $7.4 \pm 0.1$  g/min and  $0.6 \pm 0.03$  g/min,  
 314 respectively, and the natural gas leakage rate from the gas storage tank and power plant in summer  
 315 were  $1.2 \pm 0.04$  g/min and  $2.1 \pm 0.07$  g/min, respectively. The natural gas leakage rate near the  
 316 petrochemical plant was  $0.6 \pm 0.04$  g/min, which was lower than the results of Ars et al., (2020) on  
 317 the leakage rates of Toronto's natural gas distribution network (3.52–10.56 g/min), but they noted  
 318 that Well's method underestimated the leakage rate because it ignored smaller concentration  
 319 enhancements. A significant uncertainty in this method lies in the distance between the leakage point  
 320 and the vehicle; unfortunately, determining the distance between the two points in practical  
 321 operation is difficult, which may confound the estimation of methane leakage. Therefore, sufficient  
 322 mobile experiments should be conducted in subsequent work to accurately calculate natural gas  
 323 leakage in Beijing.

324



325

326 Figure 4 CH<sub>4</sub> enhancement concentration distribution map based on vehicle observations (a, c  
 327 show storage tanks and thermal power plants in winter; b, d show storage tanks and thermal power  
 328 plants in summer; e shows petrochemical plants; f shows waste disposal station; and the red box  
 329 represents high leakage value, [the map is from Google earth: https://earth.google.com/\)](https://earth.google.com/))



330  
 331 Figure 5 Fitting of the CO<sub>2</sub> and CH<sub>4</sub> concentration enhancement values (a, c show the fitting  
 332 results for the gas storage tanks and power plants in winter; b, d show the fitting results for the gas  
 333 storage tanks and power plants in summer; e shows the petrochemical plants; and f shows the  
 334 waste disposal stations. Different fitting lines represent various leakage sources.)  
 335

#### 336 4.2 Climatic effects of natural gas (NG) losses and their impact on carbon neutrality

337 Based on the natural gas consumption and flux data for the flux source area, the estimated  
 338 upper limit of the natural gas leakage rate in Beijing reached 1.12 %  $\pm$  0.22 % (Text. S5), and the  
 339 lower limit of natural gas leakage in Beijing was estimated to be 0.82 % considering the emissions  
 340 from biogenic sources (Text. S6). If the CH<sub>4</sub> fluxes were attributable solely to pipeline leakage  
 341 processes, the CH<sub>4</sub> fluxes should remain relatively stable throughout the day without significant  
 342 diurnal variations, given the constant pressure in urban pipeline pressures. However in our  
 343 observations, the CH<sub>4</sub> fluxes exhibited pronounced diurnal patterns and their spatial distribution  
 344 positively correlated with natural gas consumption. This indicates that CH<sub>4</sub> emissions in Beijing  
 345 originate predominantly from consumption-oriented leakage processes. Consequently, as natural  
 346 gas consumption surges during winter heating periods, CH<sub>4</sub> emissions from these processes (e.g.,

347 fugitive emissions from electrical devices) also increase. As a result, the ratio of emissions to  
348 consumption (leakage rate) remains relatively stable. Thus, the CH<sub>4</sub> leakage rate measured in  
349 summer is representative of year-round leakage rate of natural gas.

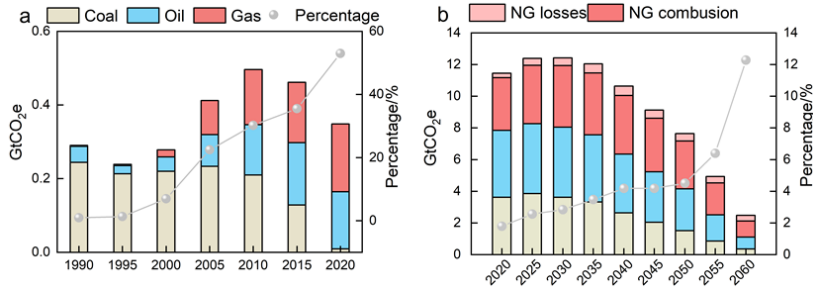
350 Our measured leakage rate was lower than the value of 2.07 % calculated based on the purchase  
351 and sales statistics and the statistical mean value of 1.1 %–1.65 % reported by the American  
352 Petroleum Institute (<https://www.api.org/>). Nevertheless, the contributions of CH<sub>4</sub> to climate  
353 warming are 8.37 % and 23.17 % of those of CO<sub>2</sub> at the 100- and 20-year scales, respectively,  
354 according to the determined CO<sub>2</sub> and CH<sub>4</sub> fluxes and the GWP of methane. With the arrival of the  
355 winter heating season, climate forcing will further increase on a yearly scale. Assuming that the  
356 natural gas consumption in Beijing during the heating season is 5 times greater than that during the  
357 other seasons (according to Beijing Gas in 2019), that oil consumption does not significantly  
358 fluctuate throughout the year and that both the CO<sub>2</sub> and CH<sub>4</sub> fluxes are positively correlated with  
359 fossil fuel consumption and natural gas leakage, the climate forcing effect of natural gas leakage in  
360 2022 was 11.47 % on a 100-year scale and could reach as high as 31.56 % on a 20-year scale.  
361 However, when the same amount of heat is generated, the use of natural gas could yield CO<sub>2</sub>  
362 emission reductions of 50 % relative to coal and of only approximately 30 % relative to oil.  
363 Therefore, the reduction in greenhouse gas emissions resulting from natural gas combustion  
364 compared with that resulting from the combustion of other fossil fuels may be offset by the climate  
365 forcing effect of CH<sub>4</sub> leakage in the short term, making it difficult for natural gas to become a  
366 transitional energy source for energy transition.

367 To assess the impact of natural gas leakage on carbon peak and carbon neutrality bas  
368 ed on our quantified leakage rate, scaling the Beijing-derived leakage rate to a national le  
369 vel is needed. However, due to the absence of leakage rate data from other cities, we can  
370 provide only a rough estimate based on available data as follows: according to the 14th  
371 Five-Year Plan for National Urban Infrastructure Development (<https://www.gov.cn/zhengce/>  
372 zhengceku/2022-07/31/5703690/files/d4ebd608827e41138701d06fe6133cdb.pdf), cities in Chin  
373 a are divided into three categories—major cities (natural gas penetration rate  $\geq$ 85 %), med  
374 ium cities (natural gas penetration rate  $\geq$ 75 %), and small cities (natural gas penetration ra  
375 te  $\geq$ 60 %). The China Gas Development Report 2023 further supplements pipeline coverag

带格式的: 允许文字在单词中间换行

376 e progress(<https://www.emerinfo.cn/download/zgtrqfzbg2003001.pdf>), indicating that large citi  
377 es and developed regions (e.g., Beijing, the Yangtze River Delta, the Pearl River Delta) a  
378 ccounted for approximately 30 %–40 % of the national pipeline length in 2022, here set a  
379 t 35 %. Small/medium cities constituted 60 %–70 % of the total pipeline length, here set  
380 at 65 %. A study based on Bayesian network modeling revealed that leakage probabilities  
381 in small/medium cities are 1.8 times higher than those in major cities (95% CI: 1.6–2.0)  
382 (Gao et al., 2024). Consequently, the national leakage rate was calculated as 1.7 % (95 %  
383 CI: 1.57 %–1.85 %)= $0.35 \times 1.12 \% + 0.65 \times 1.12 \% \times 1.8$ (95 % CI:1.6–2.0).

384 Then we adopted the results of the Global Climate Governance Strategy and China's Carbon  
385 Neutrality Path Outlook(Wang et al., 2021), which indicates that CO<sub>2</sub> emissions in China under the  
386 carbon neutrality scenario reach approximately 2.1 Gt. We calculated CH<sub>4</sub> leakage in the  
387 corresponding year based on the natural gas consumption level under the future scenario of the  
388 China Energy Outlook 2060 (SINOPEC 2021)(Economics-and-Development-Research-Institute,  
389 2021). All of the calculation results were converted CO<sub>2</sub> equivalents (CO<sub>2</sub>e) according to the GWP  
390 on a 20-year scale (Figure 6b). After taking into account the natural gas leakage process, the CO<sub>2</sub>e  
391 in China will still peak by 2030. However, the CO<sub>2</sub>e resulting from natural gas leakage will reach  
392 0.37 Gt (95 % CI: 0.34 Gt–0.40 Gt) in 2060, compared to 0.26 Gt previously. This accounts for  
393 approximately 16.6 % (95 % CI: 15.4 %–17.9 %) of the total CO<sub>2</sub> emissions (excluding natural gas  
394 leakage) and 35.9 % (95 % CI: 33.2 %–38.8 %) of the total CO<sub>2</sub> emissions from natural gas  
395 combustion, which is comparable to the CO<sub>2</sub> emissions from coal combustion (0.35 Gt). Since  
396 natural carbon sinks do not show significant short-term fluctuations, the future increase in carbon  
397 sinks will mainly rely on carbon capture and storage (CCS) technology. Given the current estimated  
398 CO<sub>2</sub> capture rate of CCS technology (0.1 Gt/year, as estimated by the China Energy Outlook 2060  
399 (SINOPEC 2021)), the achievement of carbon neutrality in China will likely be delayed by nearly  
400 three to four years. Therefore, when determining future natural gas consumption levels, it is  
401 necessary to both consider the leakage effects of natural gas and utilize carbon modeling.



402  
403 Figure 6 Terminal consumption of coal, oil, and natural gas and their proportions from 1990 to  
404 2020(a) Since diesel-powered trucks are allowed only at night on the Fifth Ring Road and  
405 kerosene, which is used mainly in aviation and is not included in the flux source area, oil mainly  
406 comprises gasoline in this case), CO<sub>2</sub> equivalent from coal, oil and natural gas (losses and  
407 combustion) in the future scenario (estimated by China Energy Outlook 2060 released by  
408 SINOPEC in 2021), and CO<sub>2</sub> equivalent of natural gas leakage as a proportion of natural gas (NG)  
409 combustion emissions(b)

#### 411 4.3 Policy implications

412 Our observations revealed a strong correlation between CH<sub>4</sub> emissions and natural gas  
413 consumption in terms of both their daily variations and spatial distributions, that is to say, the  
414 terminal consumption process drive natural gas leakage in Beijing. Liu et al., (2023) established a  
415 bottom-up emission inventory and reported that the terminal use process in Beijing accounts for 80 %  
416 of the total methane emissions in the entire natural gas supply chain. Therefore, the Chinese  
417 government may need to expand the detection of pipeline leakage to the entire natural gas industry  
418 chain.

419 Notably, existing grid-based inventory products also exhibit significant uncertainty in terms of  
420 methane sources. The extracted inventory originates from the Emissions Database for Global  
421 Atmospheric Research (EDGAR) (<https://edgar.jrc.ec.europa.eu/EDGARv8.0>). Although the mean  
422 methane flux (126.34 nmol·m<sup>-2</sup>·s<sup>-1</sup>) within the source area is close to our results, the terminal use  
423 process accounts for only approximately 13 % of the annual methane emissions, suggesting that  
424 many potential urban methane sources could have been missed, which should be considered in  
425 inventory refinement in the future.

426 In addition, minimizing the methane leakage rate could ensure the early realization of carbon  
427 neutrality in China. Although methane emission control has been included in the agenda for the first

428 time in the Methane Emission Control Action Plan promulgated in 2023, which clearly highlights  
429 the need to promote the application of leak detection and repair technology and to enhance the  
430 comprehensive recovery and utilization of methane, methane leakage standards have not been  
431 updated. Previous methane leakage standards focused only on controlling the amount of methane  
432 leakage from a safe perspective, thereby ignoring the climate effects of natural gas leakage. China  
433 must urgently develop a strict and detailed set of natural gas leakage standards.

#### 434 **4.4 Limitations**

435 The flux discussed in this study is net flux, which means considering both positive flux and  
436 negative flux simultaneously. It should be noted that for flux values close to zero (particularly the  
437 negative values observed at night), we have retained all the data points without employing a filtering  
438 method based on the statistics of instrument white noise. Whereas a more rigorous approach would  
439 be to model these fluxes fluctuating around zero as white noise and establish a statistical significance  
440 threshold based on this. Discarding all values within this threshold (including slightly positive and  
441 slightly negative ones) could effectively reduce noise-induced bias, although at the cost of data  
442 coverage. The development and application of such objective, instrument-physics-based filtering  
443 criteria represent an important direction for future research to enhance the quality and reliability of  
444 flux data, particularly under low-turbulence conditions.

445 For the source analysis of CO<sub>2</sub> and CH<sub>4</sub>, we did not consider the impact of long-distance  
446 transportation. However, this impact may not be completely ignored. For example, in the upwind  
447 area of Beijing, Shanxi Province is a high-intensity area of anthropogenic pollutant emissions, where  
448 the actual lifespan of local CO may be significantly shortened due to the influence of local OH  
449 concentration. The CO<sub>2</sub> produced by CO there is not insignificant(Li et al., 2025), which may also  
450 be one of the sources of local CO<sub>2</sub> in Beijing. Therefore, it is necessary to combine regional chemical  
451 transport models to more accurately quantify the impact of local chemical coupling in future flux  
452 research.

453 When quantifying CH<sub>4</sub> leakage from different natural gas facilities, we adopted a quantile  
454 based deterministic method to separate background concentration from enhanced signals, and  
455 mainly explored the sensitivity brought by algorithm parameter selection. However, this framework  
456 has a fundamental limitation: it fails to incorporate the inherent observational uncertainty of

带格式的: 字体: (默认) Times New Roman, (中文) Times New Roman

带格式的: 正文, 缩进: 首行缩进: 2 字符

带格式的: 字体: (中文) 等线

457 background concentration and on-site observed concentration into a unified probabilistic analysis.  
458 The observation error of background value and enhanced signal are coupled (Lu et al., 2025; Zheng  
459 et al., 2025), they will propagate together, and significantly affect the final uncertainty interval of  
460 emission estimation. Our current sensitivity analysis can only be one step in such comprehensive  
461 uncertainty quantification work (i.e. identifying sensitivity to parameter selection), and future work  
462 should focus on: (1) systematically quantifying the instrument errors used in this study; (2)  
463 integrating these prior uncertainties into the inversion process of emissions using probabilistic  
464 frameworks such as Bayesian inference or error propagation models; (3) expanding the emission  
465 estimation from a single 'best estimate' to a probability distribution that includes confidence  
466 intervals.

467 Although we estimated the impact of natural gas leaks on China's carbon neutrality process,  
468 the national-scale extrapolation of the natural gas leakage rate conducted in this study carried  
469 substantial uncertainty. Our approach, which relied on a simplified scaling method due to data  
470 availability constraints, may fail to account for strong regional heterogeneities in natural gas  
471 consumption patterns and infrastructure conditions. As highlighted by recent literatures (Qin et al.,  
472 2023; Hu et al., 2024), such scaling methods can systematically miss substantial emission sources  
473 in specific regions (e.g., industrial hubs like Shanxi Province). Therefore, our national estimate  
474 should be interpreted as a rough attempt.

## 475 **5. SUMMARY AND ConclusionsONCLUSIONS and outlooks**

476 This study utilized the eddy covariance method to measure CO<sub>2</sub> and CH<sub>4</sub> fluxes at 220-m height  
477 in urban Beijing, providing critical insights into surface-atmosphere exchanges of greenhouse gases  
478 in the region. First, urban areas unequivocally act as net sources of both CO<sub>2</sub> and CH<sub>4</sub>. The daily  
479 mean fluxes were  $12.21 \pm 1.75 \text{ } \mu\text{mol} \cdot \text{m}^{-2} \cdot \text{s}^{-1}$  for CO<sub>2</sub> and  $95.54 \pm 18.92 \text{ } \text{nmol} \cdot \text{m}^{-2} \cdot \text{s}^{-1}$  for CH<sub>4</sub>, with  
480 daytime emissions significantly exceeding nighttime levels, highlighting the importance of  
481 anthropogenic influences.

482 Although diurnal variation patterns differed slightly between CO<sub>2</sub> and CH<sub>4</sub> fluxes, their strong  
483 correlation indicates shared dominant sources. Spatial distribution analysis revealed high  
484 consistency between both fluxes and natural gas consumption patterns, confirming natural gas as a  
485 common source. With Beijing's energy restructuring, natural gas has become the dominated

带格式的: 字体: (中文) 等线

486 terminal energy consumption. Its combustion releases substantial CO<sub>2</sub>, while leakage processes emit  
487 CH<sub>4</sub>, as validated by mobile observations detecting CH<sub>4</sub> fugitive emissions during production,  
488 storage and use stages. Although biogenic sources could contribute to CH<sub>4</sub> emissions, they account  
489 for at most 27 % of total CH<sub>4</sub> fluxes in the source area, ruling out the view that biological sources  
490 dominate both emissions. Attributing all CH<sub>4</sub> emissions to natural gas usage, the upper leakage rate  
491 of natural gas in Beijing was calculated as 1.12 % ± 0.22 %.

492 The CH<sub>4</sub> emissions from natural gas will exacerbate climate warming. Calculated flux results  
493 showed that the contribution of CH<sub>4</sub> to climate warming on a century and 20-year scale can reach  
494 as high as 8.37 % and 23.17 % of CO<sub>2</sub>, respectively. On the basis of predicted energy report and  
495 calculated leakage rate, it is roughly predicted that natural gas leakage will delay China's realization  
496 of carbon neutrality, which necessitates urgent attention to mitigate associated climate effects.

497 Future work should prioritize the development of more granular, bottom-up inventories based on  
498 province-level activity data and infrastructure surveys to achieve a more accurate and robust  
499 assessment of China's overall natural gas leakage.

带格式的: 字体: Times New Roman

## 500 SUPPORTING INFORMATION

501 Details about the Beijing Meteorological Tower, eddy observation system and navigation  
502 observation station, daily summer variation in CO<sub>2</sub> flux from 2009 to 2017, total consumption,  
503 electricity inflow and the proportion of natural gas in total energy consumption from 2013-2022,  
504 spatial distribution of CO<sub>2</sub> and CH<sub>4</sub> fluxes with wind speed and direction, grid distribution of natural  
505 gas consumption in Beijing, calculation methods of the flux source area and natural gas leakage rate,  
506 uncertainty analysis of flux calculation, estimation of non-natural gas sources

## 507 ACKNOWLEDGMENTS

508 This work was supported by the National Key R&D Program of China (2023YFC3706103), the  
509 Strategic Priority Research Program of the Chinese Academy of Sciences (XDB0760200), the  
510 Beijing Municipal Natural Science Foundation (No. 8222075), the Youth Cross Team Scientific  
511 Research Project of the Chinese Academy of Sciences (No. JCTD-2021-10) and the S&T Program  
512 of Hebei (22373903D).

## 513 DATA AVAILABILITY

514 All the data generated or analyzed in this study are included in the published article and are available

515 from the authors upon reasonable request.

## 516 COMPETING INTERESTS

517 The authors declare that they have no competing interests.

## 518 REFERENCES

519 Ars, S., Vogel, F., Arrowsmith, C., Heerah, S., Knuckey, E., Lavoie, J., Lee, C., Pak, N. M., Phillips,  
520 J. L., and Wunch, D.: Investigation of the Spatial Distribution of Methane Sources in the  
521 Greater Toronto Area Using Mobile Gas Monitoring Systems, *Environ. Sci. Technol.*, 54,  
522 15671-15679, <http://doi.org/10.1021/acs.est.0c05386>, 2020.

523 Barlow, J. F.: Progress in observing and modelling the urban boundary layer, *Urban Climate*, 10,  
524 216-240, <http://doi.org/10.1016/j.uclim.2014.03.011>, 2014.

525 Chen, Z., Jacob, D. J., Nesser, H., Sulprizio, M. P., Lorente, A., Varon, D. J., Lu, X., Shen, L., Qu,  
526 Z., Penn, E., and Yu, X.: Methane emissions from China: a high-resolution inversion of  
527 TROPOMI satellite observations, *Atmos. Chem. Phys.*, 22, 10809-10826,  
528 <http://doi.org/10.5194/acp-22-10809-2022>, 2022.

529 Cheng, X. L., Liu, X. M., Liu, Y. J., and Hu, F.: Characteristics of CO<sub>2</sub> concentration and flux in the  
530 Beijing urban area, *J. Geophys. Res.-Atmos.*, 123, 1785-1801,  
531 <http://doi.org/10.1002/2017JD027409>, 2018.

532 Cusworth, D. H., Duren, R. M., Ayasse, A. K., Jiorle, R., Howell, K., Aubrey, A., Green, R. O.,  
533 Eastwood, M. L., Chapman, J. W., Thorpe, A. K., Heckler, J., Asner, G. P., Smith, M. L., Thoma,  
534 E., Krause, M. J., Heins, D., and Thorneloe, S.: Quantifying methane emissions from United  
535 States landfills, *Science*, 383, 1499-1504, <http://doi.org/10.1126/science.adi7735>, 2024.

536 Cusworth, D. H., Jacob, D. J., Sheng, J.-X., Benmergui, J., Turner, A. J., Brandman, J., White, L.,  
537 and Randles, C. A.: Detecting high-emitting methane sources in oil/gas fields using satellite  
538 observations, *Atmos. Chem. Phys.*, 18, 16885-16896, <http://doi.org/10.5194/acp-18-16885-2018>, 2018.

539 Donato, A., Conte, M., Grasso, F. M., and Contini, D.: Seasonal and diurnal behaviour of size  
540 segregated particles fluxes in a suburban area, *Atmos. Environ.*, 219, 117052,  
541 <http://doi.org/10.1016/j.atmosenv.2019.117052>, 2019.

542 Duren, R. M., Thorpe, A. K., Foster, K. T., Rafiq, T., Hopkins, F. M., Yadav, V., Bue, B. D.,  
543 Thompson, D. R., Conley, S., Colombi, N. K., Frankenberg, C., McCubbin, I. B., Eastwood,  
544 M. L., Falk, M., Herner, J. D., Croes, B. E., Green, R. O., and Miller, C. E.: California's methane  
545 super-emitters, *Nature*, 575, 180-184, <http://doi.org/10.1038/s41586-019-1720-3>, 2019.

546 Economics-and-Development-Research-Institute: World and China Energy Outlook 2060,  
547 <https://www.docin.com/p-2955292161.html>, 2021.

548 Environmental-Protection-Agency: Understanding global warming potentials,  
549 <https://www.epa.gov/ghgemissions/understandingglobal-warming-potentials>, last accessed: 22  
550 Oct. 2024.

551 Fan, S. M., Wofsy, S. C., Bakwin, P. S., Jacob, D. J., and Fitzjarrald, D. R.: Atmosphere–biosphere  
552 exchange of CO<sub>2</sub> and O<sub>3</sub> in the central Amazon Forest, *JGR: Atmospheres*, 95, 16851-16864,  
553 <http://doi.org/10.1029/JD095iD10p16851>, 2012.

554 Frankenberg, C., Thorpe, A. K., Thompson, D. R., Hulley, G., Kort, E. A., Vance, N., Borchardt, J.,

555

556 Krings, T., Gerilowski, K., Sweeney, C., Conley, S., Bue, B. D., Aubrey, A. D., Hook, S., and  
557 Green, R. O.: Airborne methane remote measurements reveal heavy-tail flux distribution in  
558 Four Corners region, *Proc. Natl. Acad. Sci. U. S. A.*, 113, 9734-9739,  
559 <http://doi.org/10.1073/pnas.1605617113>, 2016.

560 Gao, S., Tian, W., and Wang, C.: A method, system, equipment, and medium for determining  
561 methane leakage in a natural gas pipeline network: 202410249186, in Chinese, 2024.

562 Gioli, B., Toscano, P., Lugato, E., Matese, A., Miglietta, F., Zaldei, A., and Vaccari, F. P.: Methane  
563 and carbon dioxide fluxes and source partitioning in urban areas: the case study of Florence,  
564 Italy, *Environ Pollut*, 164, 125-131, <http://doi.org/10.1016/j.envpol.2012.01.019>, 2012.

565 Helfter, C., Tremper, A. H., Halios, C. H., Kotthaus, S., Björkegren, A., Grimmond, C. S. B., Barlow,  
566 J. F., and Nemitz, E.: Spatial and temporal variability of urban fluxes of methane, carbon  
567 monoxide and carbon dioxide above London, UK, *Atmos. Chem. Phys.*, 16, 10543-10557,  
568 <http://doi.org/10.5194/acp-16-10543-2016>, 2016.

569 [Hu, W., Qin, K., Lu, F., Li, D., and Cohen, J. B.: Merging TROPOMI and eddy covariance](#) 带格式的: 正文, 缩进: 左侧: 0 厘米, 悬挂缩进: 2 字符  
570 [observations to quantify 5-years of daily CH<sub>4</sub> emissions over coal-mine dominated region, Int.](#)  
571 [J. Coal Sci. Technol.](#), 11, 56, <https://doi.org/10.1007/s40789-024-00700-1>, 2024. 带格式的: 检查拼写和语法

572 Hurry, J., Risk, D., Lavoie, M., Brooks, B.-G., Phillips, C. L., and Göckede, M.: Atmospheric  
573 monitoring and detection of fugitive emissions for Enhanced Oil Recovery, *Int. J. Greenh. Gas*  
574 Con., 45, 1-8, <http://doi.org/10.1016/j.ijggc.2015.11.031>, 2016.

575 Kaimal, J. C., and Finnigan, J. J.: Atmospheric boundary layer flows: their structure and  
576 measurement. New York: Oxford University Press, 1994.

577 Kaimal, J. C., Wyngaard, J. C., Izumi, Y., and Coté, O. R.: Spectral characteristics of surface-layer  
578 turbulence, *Quart. J. R. Met. Soc.*, 98, 563-589, <http://doi.org/10.1002/qj.49709841707>, 1972.

579 Kemfert, C., Präger, F., Brauner, I., Hoffart, F. M., and Brauers, H.: The expansion of natural gas  
580 infrastructure puts energy transitions at risk, *Nature Energy*, 7, 582-587,  
581 <http://doi.org/10.1038/s41560-022-01060-3>, 2022.

582 Kljun, N., Calanca, P., Rotach, M. W., and Schmid, H. P.: A Simple Parameterisation for Flux  
583 Footprint Predictions, *Boundary-Layer Meteorology*, 112, 503-523,  
584 <http://doi.org/10.1023/b:Boun.0000030653.71031.96>, 2004.

585 Lamb, B. K., McManus, J. B., Shorter, J. H., Kolb, C. E., Mosher, B., Harriss, R. C., Allwine, E.,  
586 Blaha, D., Howard, T., Guenther, A., Lott, R. A., Siverson, R., Westburg, H., and Zimmerman,  
587 P.: Development of atmospheric tracer methods to measure methane emissions from natural  
588 gas facilities and urban areas, *Environ. Sci. Technol.*, 29, 1468-1479,  
589 <http://doi.org/10.1021/es00006a007>, 1995.

590 Lee, X.: *Handbook of micrometeorology: A Guide for surface Flux Measurement and Analysis*.  
591 New York: Kluwer Academic Publishers, 2004.

592 [Li, X., Cohen, J. B., Tiwari, P., Wu, L., Wang, S., He, Q., Yang, H., and Qin, K.: Space-based](#) 带格式的: 正文, 缩进: 左侧: 0 厘米, 悬挂缩进: 2 字符  
593 [inversion reveals underestimated carbon monoxide emissions over Shanxi, Commun. Earth](#)  
594 [Environ.](#), 6, 357, <https://doi.org/10.1038/s43247-025-02301-5>, 2025. 带格式的: 字体: +西文正文 (等线)

595 Liu, H. Z., Feng, J. W., Järvi, L., and Vesala, T.: Four-year (2006–2009) eddy covariance  
596 measurements of CO<sub>2</sub> flux over an urban area in Beijing, *Atmos. Chem. Phys.*, 12, 7881-7892,  
597 <http://doi.org/10.5194/acp-12-7881-2012>, 2012.

598 Liu, S., Liu, K., Wang, K., Chen, X., and Wu, K.: Fossil-Fuel and Food Systems Equally Dominate

599        Anthropogenic Methane Emissions in China, *Environ. Sci. Technol.*, 57, 2495-2505,  
600        <http://doi.org/10.1021/acs.est.2c07933>, 2023.

601        Liu, Z., Liu, Z., Song, T., Gao, W., Wang, Y., Wang, L., Hu, B., Xin, J., and Wang, Y.: Long-term  
602        variation in CO<sub>2</sub> emissions with implications for the interannual trend in PM(2.5) over the last  
603        decade in Beijing, China, *Environ. Pollut.*, 266, 115014,  
604        <http://doi.org/10.1016/j.envpol.2020.115014>, 2020.

605        [Lu, F., Qin, K., Cohen, J. B., He, Q., Tiwari, P., Hu, W., Ye, C., Shan, Y., Xu, Q., Wang, S., and Tu, Q.: Surface-observation-constrained high-frequency coal mine methane emissions in Shanxi, China, reveal more emissions than inventories, consistent with satellite inversion, Atmos. Chem. Phys., 25, 5837-5856, https://doi.org/10.5194/acp-25-5837-2025, 2025.](#)        带格式的: 正文, 缩进: 左侧: 0 厘米, 悬挂缩进: 2 字符

606        [Qin, K., Hu, W., He, Q., Lu, F., and Cohen, J. B.: Individual coal mine methane emissions constrained by eddy covariance measurements: low bias and missing sources, Atmos. Chem. Phys., 24, 3009-3028, https://doi.org/10.5194/acp-24-3009-2024, 2024.](#)        带格式的: 检查拼写和语法

607        Pawlak, W., and Fortuniak, K.: Eddy covariance measurements of the net turbulent methane flux in  
608        the city centre – results of 2-year campaign in Łódź, Poland, *Atmos. Chem. Phys.*, 16, 8281-8294, <http://doi.org/10.5194/acp-16-8281-2016>, 2016.

609        Mauder, M., and Foken, T.: Documentation and Instruction Manual of the Eddy Covariance  
610        Software Package TK2, *Proc. R. Soc. Med.*, 26, 42-46, <http://doi.org/10.5281/zenodo.20349>,  
611        2004.

612        Moncrieff, J. B., Malhi, Y., and Leuning, R.: The propagation of errors in long-term measurements  
613        of land - atmosphere fluxes of carbon and water, *Global Change Biology*, 2, 231-240,  
614        <http://doi.org/10.1111/j.1365-2486.1996.tb00075.x>, 1996.

615        Pu, W., Sheng, J., Tian, P., Huang, M., Liu, X., Collett Jr, J.L., Li, Z., Zhao, X., He, D., Dong, F.:  
616        On-road mobile mapping of spatial variations and source contributions of ammonia in Beijing,  
617        China, *Sci. Total Environ.*, 864, 160869, 2023.

618        [Qin, K., Hu, W., He, Q., Lu, F., and Cohen, J. B.: Individual coal mine methane emissions constrained by eddy covariance measurements: low bias and missing sources, Atmos. Chem. Phys., 24, 3009-3028, https://doi.org/10.5194/acp-24-3009-2024, 2024.](#)

619        Sargent, M. R., Floerchinger, C., McKain, K., Budney, J., Gottlieb, E. W., Hutyra, L. R., Rudek, J.,  
620        and Wofsy, S. C.: Majority of US urban natural gas emissions unaccounted for in inventories,  
621        *Proc. Natl. Acad. Sci. U. S. A.*, 118, e2105804118, <http://doi.org/10.1073/pnas.2105804118>,  
622        2021.

623        Schiferl, L.D., Hallward-Driemeier, A., Zhao, Y., Toledo-Crow, R., and Commane, R.: Missing  
624        wintertime methane emissions from New York City related to combustion, *EGUphere*, 2025,  
625        1-28, <https://doi.org/10.5194/eguphere-2025-345>, 2025.

626        Seneviratne, S. I., Rogelj, J., Seferian, R., Wartenburger, R., Allen, M. R., Cain, M., Millar, R. J.,  
627        Ebi, K. L., Ellis, N., Hoegh-Guldberg, O., Payne, A. J., Schleussner, C. F., Tschakert, P., and  
628        Warren, R. F.: The many possible climates from the Paris Agreement's aim of 1.5 degrees C  
629        warming, *Nature*, 558, 41-49, <http://doi.org/10.1038/s41586-018-0181-4>, 2018.

630        Shen, L., Jacob, D. J., Gautam, R., Omara, M., Scarpelli, T. R., Lorente, A., Zavala-Araiza, D., Lu,  
631        X., Chen, Z., and Lin, J.: National quantifications of methane emissions from fuel exploitation  
632        using high resolution inversions of satellite observations, *Nat. Commun.*, 14, 4948,  
633        <http://doi.org/10.1038/s41467-023-40671-6>, 2023.

634        Sherwin, E. D., Rutherford, J. S., Zhang, Z., Chen, Y., Wetherley, E. B., Yakovlev, P. V., Berman, E.  
635        S. F., Jones, B. B., Cusworth, D. H., Thorpe, A. K., Ayasse, A. K., Duren, R. M., and Brandt,  
636        A. R.: US oil and gas system emissions from nearly one million aerial site measurements,  
637        *Nature*, 627, 328-334, <http://doi.org/10.1038/s41586-024-07117-5>, 2024.

638

639

640

641

642

643 Sun, W., Deng, L., Wu, G., Wu, L., Han, P., Miao, Y., and Yao, B.: Atmospheric Monitoring of  
644 Methane in Beijing Using a Mobile Observatory, *Atmosphere*, 10, 554,  
645 <http://doi.org/10.3390/atmos10090554>, 2019.

646 Vickers, D., and Mahrt, L.: Quality Control and Flux Sampling Problems for Tower and Aircraft  
647 Data, *J. Atmos. Oceanic Technol.*, 14, 512-526, [http://doi.org/10.1175/1520-0426\(1997\)014<0512:Qcafsp>2.0.Co;2](http://doi.org/10.1175/1520-0426(1997)014<0512:Qcafsp>2.0.Co;2), 1997.

648 Wang, P., Zhou, W., Xiong, X., Wu, S., Niu, Z., Cheng, P., Du, H., and Hou, Y.: Stable carbon  
649 isotopic characteristics of fossil fuels in China, *Sci. Total. Environ.*, 805, 150240,  
650 <http://doi.org/10.1016/j.scitotenv.2021.150240>, 2022.

651 Wang, P., Zhou, W., Xiong, X., Wu, S., Niu, Z., Yu, Y., Liu, J., Feng, T., Cheng, P., Du, H., Lu, X.,  
652 Chen, N., and Hou, Y.: Source Attribution of Atmospheric CO<sub>2</sub> Using <sup>14</sup>C and <sup>13</sup>C as Tracers  
653 in Two Chinese Megacities During Winter, *JGR: Atmospheres*, 127, e2022JD036504,  
654 <http://doi.org/10.1029/2022jd036504>, 2022.

655 Wang, Y., Guo, C. H., Chen, X. J., Jia, L. Q., Guo, X. N., Chen, R. S., and Wang, H. D.: Global  
656 climate governance strategies and prospects for China's carbon neutrality path. *Forecasting  
657 And Prospects Research Report*, 2021.

658 Webb, E. K., Pearman, G. I., and Leuning, R.: Correction of flux measurements for density effects  
659 due to heat and water vapour transfer, *Q. J. R. Meteorolog. Soc.*, 106, 85-100,  
660 <http://doi.org/10.1002/qj.49710644707>, 2007.

661 Weller, Z. D., Roscioli, J. R., Daube, W. C., Lamb, B. K., Ferrara, T. W., Brewer, P. E., and von  
662 Fischer, J. C.: Vehicle-Based Methane Surveys for Finding Natural Gas Leaks and Estimating  
663 Their Size: Validation and Uncertainty, *Environ. Sci. Technol.*, 52, 11922-11930,  
664 <http://doi.org/10.1021/acs.est.8b03135>, 2018.

665 Weller, Z. D., Yang, D. K., and von Fischer, J. C.: An open source algorithm to detect natural gas  
666 leaks from mobile methane survey data, *PLoS One*, 14, e0212287,  
667 <http://doi.org/10.1371/journal.pone.0212287>, 2019.

668 Wunch, D., Toon, G. C., Hedin, J. K., Vizenor, N., Roehl, C. M., Saad, K. M., Blavier, J.-F. L.,  
669 Blake, D. R., and Wennberg, P. O.: Quantifying the loss of processed natural gas within  
670 California's South Coast Air Basin using long-term measurements of ethane and methane,  
671 *Atmos. Chem. Phys.*, 16, 14091-14105, <http://doi.org/10.5194/acp-16-14091-2016>, 2016.

672 Zheng, B., Cohen, J. B., Lu, L., Hu, W., Tiwari, P., Lolli, S., Garzelli, A., Su, H., and Qin, K.: How  
673 can we trust TROPOMI based Methane Emissions Estimation: Calculating Emissions over  
674 Unidentified Source Regions, EGUsphere [preprint], <https://doi.org/10.5194/egusphere-2025-1446>, 2025.

675

676 Zöll, U., Brümmer, C., Schrader, F., Ammann, C., Ibrom, A., Flechard, C. R., Nelson, D. D.,  
677 Zahniser, M., and Kutsch, W. L.: Surface-atmosphere exchange of ammonia over peatland  
678 using QCL-based eddy-covariance measurements and inferential modeling, *Atmos. Chem.  
679 Phys.*, 16, 11283-11299, <http://doi.org/10.5194/acp-16-11283-2016>, 2016.

680

带格式的: 正文, 缩进: 左侧: 0 厘米, 悬挂缩进: 2 字符

带格式的: 检查拼写和语法